INSTITUTE OF PHYSICS PUBLISHING JOURNAL OF PHYSICS B: ATOMIC, MOLECULAR AND OPTICAL PHYSICS

J. Phys. B: At. Mol. Opt. Phys. **34** (2001) 3205–3220 PII: S0953-4075(01)19211-4

Electron spectra from singlet and triplet states of Ne^{6+**} produced by low energy Ne^{8+} + He, Ne and Ar collisions

S Kitazawa[1], H Ida[2], Y Matsui[2], T Takayanagi[2], K Wakiya[2], K Iemura[3], S Ohtani[3], H Suzuki[3], Y Kanai[4] and U I Safronova[5]

[1] Japan Atomic Energy Research Institute (JAERI), Tokai, Ibaraki 319-1195, Japan
[2] Department of Physics, Sophia University, Chiyoda-ku, Tokyo 102-8554, Japan
[3] Institute for Laser Science (ILS), University of Electro-Communications, Chofu, Tokyo 182-8585, Japan
[4] RIKEN, 2-1 Hirosawa, Wako, Saitama 351-0198, Japan
[5] Department of Physics, University of Notre Dame, Notre Dame, IN 46556, USA

Received 20 November 2000, in final form 24 May 2001
Published 1 August 2001
Online at stacks.iop.org/JPhysB/34/3205

Abstract

Ejected electron spectra from the singlet and triplet states of doubly excited $Ne^{6+**}(1s^2 2pnl)$, $Ne^{6+**}(1s^2 3l3l')$ and $Ne^{6+**}(1s^2 3l4l')$ ions, produced by 80 keV $Ne^{8+}(1s^2)$ + He, Ne and Ar collisions, have been measured by means of a zero-degree electron spectroscopy. Only singlet states were observed when the target was He. In contrast, the contribution from the triplet states prevailed in the spectra for the Ne target. For the Ar target, practically no signals were observed in the energy region for the $1s^2 3lnl'$ states. Two theoretical methods, the perturbation theory (MZ code) and the multi-configurational Hartree–Fock (Cowan code) were used for identification of ejected-electron spectra. Using the (j) string analysis in the extended classical over-barrier model, we discuss the possibility of the participation of inner electrons in the process of double-electron capture by highly charged ion multi-electron target atoms.

1. Introduction

Charge transfer processes between the He-like Ne^{8+} projectile and gas targets have been investigated by some groups. Bonnet *et al* (1985) studied the single electron capture into different (nl) states of Ne^{8+} projectile from He and H_2 targets by observing x-rays. For double electron capture by Ne^{8+} ions, Mack and Niehaus (1987) analysed Ne^{8+} + He and H_2 collisions at 89.6 keV using a scheme of reaction windows. Boudjema *et al* (1991a, b) showed angular dependence of ejected electron spectra in Ne^{8+} + He and H_2 collisions for 80 keV at angles of 10°, 90° and 160°.

Recently, experiments on highly charged ion collisions are being widely investigated using electron cyclotron resonance (ECR) ion sources. We have performed a series of studies on double-electron transfer processes by means of the ejected-electron spectroscopy in the collisions of highly charged low-energy He-like ions with rare gas atoms using ECR ion sources (Kanai *et al* 1995, Nakamura *et al* 1994, 1995, Kitazawa *et al* 1997, 1998). The energy and target dependences were investigated on the population distribution of the singlet and triplet states in O^{6+} (Nakamura *et al* 1995) and N^{5+} (Kitazawa *et al* 1998) projectiles. In these works, we have shown experimentally that triplet states of doubly excited O^{4+} and N^{3+} are dominantly produced by the O^{6+} + Ne and N^{5+} + Ar collisions, respectively. We suggested for these collisions that the two electrons which have the lowest ionization potential are removed from a rare-gas atom target with the electron configuration $np^6\ ^1S$, resulting in the doubly ionized ion state $np^4\ ^3P$. We have also shown that electrons from both singlet and triplet states are detected when the reaction window for the process mentioned above does not overlap with the region where the doubly excited states concerned exist, and other processes must be taken into account in such cases. The O^{4+**} ($1s^2 3l3l'$) doubly excited state formation by O^{6+} + Ar collision is one such example (Nakamura *et al* 1995).

In this paper we report the measured energy levels of doubly excited Ne^{6+**} ions as observed experimentally in the collisions of He-like Ne^{8+} ions with He, Ne and Ar, and compare them with results of theoretical calculations. We discuss further the features of the mechanism of the double-electron transfer processes observed in collisions of Ne^{8+} with rare gases. Experimental procedures are described in section 2 and theoretical approaches in section 3. The results of the identification of peaks due to the doubly excited Ne^{6+**} ions are given in section 4. In section 5, we discuss the specific characteristics in the spectra including both the singlet and triplet states using the reaction window approach (Niehaus 1986). Finally, we summarize the paper in section 6.

2. Experimental method

We have measured the energy distributions of the ejected electrons in the electron capture collisions of Ne^{8+} projectile ions with He, Ne and Ar targets. These experiments were performed using the ECR ion source in RIKEN (Sakaue *et al* 1990, Kanai *et al* 1995). Ions were extracted from the ion sources and mass analysed by a 90° magnet, transported through a bending magnet and focused by an einzel electrostatic lens system. The ion beam was well collimated by a pair of apertures in front of a target gas cell. The gas cell is 5 cm in length and its entrance and exit apertures are 2.0 and 2.5 mm in diameter, respectively.

Ejected electrons were measured at an observation angle of 0° with respect to the beam direction by a 45° parallel plate electrostatic pre-analyser and a high energy-resolution electrostatic analyser of the simulated hemispherical type with a mean radius of 104 mm. The energy resolution of the spectrometer was typically 100 meV (FWHM). Single collision conditions were confirmed by measuring the target pressure dependence of the electron spectra. The target gas pressure in the gas cell was of the order of 10^{-3}–10^{-1} Pa, which was used as this made it possible to eliminate double collisions. The details of the experimental set-up were given in previous papers (Sakaue *et al* 1990, Kanai *et al* 1995, Kitazawa *et al* 1998).

3. Theoretical method

In table 1, we present Auger energies of $1s^2 2pnl$ states with $n = 7$–15, l = s, p, d and f for Ne^{6+} calculated using MZ code. MZ code was based on the perturbation theory method

Table 1. Coster–Kronig energy (relative to $1s^2 2s$) for $Ne^{6+}(1s^2 2pnl)$ states (eV).

Configuration	Level	$n = 7$	$n = 8$	$n = 9$	$n = 10$	$n = 11$	$n = 12$	$n = 13$	$n = 14$	$n = 15$
2p*n*s	$^3P_0$	1.7230	5.1809	7.5293	9.1965	10.4226	11.3504	12.0695	12.6380	13.0952
2p*n*s	$^3P_1$	1.7402	5.1927	7.5376	9.2026	10.4271	11.3539	12.0722	12.6401	13.0970
2p*n*s	$^3P_2$	1.9292	5.3869	7.7341	9.3959	10.6357	11.5613	12.2796	12.8480	13.3050
2p*n*s	$^1P_1$	1.9792	5.4190	7.7574	9.4180	10.6433	11.5679	12.2851	12.8523	13.3086
2p*n*p	$^3D_1$	2.0175	5.3777	7.6671	9.2966	10.4976	11.4080	12.1147	12.6740	13.1245
2p*n*p	$^3D_2$	2.0903	5.4330	7.7095	9.3294	10.5233	11.4284	12.1310	12.6873	13.1354
2p*n*p	$^1P_1$	2.0941	5.5984	7.8821	9.5091	10.7089	11.6188	12.3251	12.8843	13.3346
2p*n*p	$^3P_0$	2.2093	5.5135	7.7669	9.3720	10.5558	11.4538	12.1512	12.7037	13.1488
2p*n*p	$^3D_3$	2.2406	5.5948	7.8839	9.5108	10.7105	11.6203	12.3264	12.8854	13.3355
2p*n*p	$^3S_1$	2.2537	5.4342	7.7087	9.5444	10.7358	11.6396	12.3415	12.8975	13.3454
2p*n*d	$^3F_2$	2.2782	5.5519	7.7893	9.3849	10.5642	11.4594	12.1550	12.7064	13.1506
2p*n*p	$^3P_1$	2.3445	5.6640	7.9297	9.3278	10.5214	11.4265	12.1294	12.6858	13.1340
2p*n*p	$^3P_2$	2.3465	5.6661	7.9283	9.5426	10.7339	11.6379	12.3400	12.8962	13.3443
2p*n*d	$^3P_2$	2.3732	5.6206	7.8405	9.4310	10.5870	11.4785	12.1704	12.7189	13.1609
2p*n*f	$^3G_3$	2.3824	5.6212	7.8377	9.4207	10.5907	11.4797	12.1709	12.7192	13.1611
2p*n*f	$^3G_4$	2.4003	5.6337	7.8467	9.4275	10.5958	11.4837	12.1741	12.7217	13.1632
2p*n*f	$^3F_2$	2.4091	5.6449	7.8575	9.4359	10.6025	11.4890	12.3873	12.9342	13.3750
2p*n*f	$^3F_3$	2.4160	5.6455	7.8529	9.3335	10.5989	12.1032	12.2929	13.2353	12.7954
2p*n*d	$^3D_1$	2.4468	5.6698	7.8750	9.4508	10.6117	11.4969	12.1849	12.7305	13.1705
2p*n*p	$^1D_2$	2.4549	5.7283	7.9727	9.5751	10.7584	11.6568	12.3549	12.9081	13.3540
2p*n*d	$^3F_4$	2.4824	5.7575	7.9957	9.5929	10.7724	11.6678	12.3638	12.9153	13.3598
2p*n*d	$^1D_2$	2.5275	5.7831	8.0122	9.6043	10.7804	11.6740	12.3685	12.9192	13.3629
2p*n*f	$^1F_3$	2.5925	5.8312	8.0476	9.6307	10.8006	11.6896	12.3809	12.9291	13.3710
2p*n*f	$^3F_4$	2.5970	5.8342	8.0497	9.6322	10.8019	11.6905	12.3817	12.9297	13.3715
2p*n*d	$^3D_2$	2.6137	5.8449	8.0569	9.6373	10.8055	11.6933	12.3838	12.9313	13.3728
2p*n*d	$^3P_1$	2.6189	5.8485	8.0593	9.6392	10.8070	11.6944	12.3847	12.9319	13.3734
2p*n*d	$^3P_0$	2.6200	5.8488	8.0595	9.6390	10.8068	11.6942	12.3845	12.9318	13.3732
2p*n*f	$^3D_3$	2.6282	5.8540	8.0632	9.4327	10.5999	11.4869	12.1766	12.7238	13.1648
2p*n*f	$^1G_4$	2.6331	5.8579	8.0660	9.6441	10.8107	11.6973	12.3869	12.9339	13.3749
2p*n*f	$^3D_2$	2.6379	5.8605	8.0677	9.6451	10.8113	11.6978	12.1784	12.7251	13.1660
2p*n*f	$^3D_1$	2.6579	5.8749	8.0782	9.6530	10.8174	11.7025	12.3910	12.9371	13.3777
2p*n*p	$^1S_0$	2.6652	5.8697	8.0689	9.6430	10.8080	11.6942	12.3839	12.9309	13.3723
2p*n*f	$^1D_2$	2.6804	5.8891	8.0877	9.6597	10.8223	11.7062	12.3940	12.9395	13.3795
2p*n*d	$^1P_1$	2.8020	5.9660	8.1392	9.6958	10.8487	11.7261	12.4093	12.9515	13.3892

with Coulomb basis. In this method (the $1/Z$ method or $1/Z$-expansion method) an energy matrix is represented in the form of a $1/Z$-expansion series (Z is the nuclear charge) and the calculation of every coefficient of this series is carried out by means of the Feynman diagram technique. This method was described in detail by Safronova and Senashenko (1984) and Safronova *et al* (1996). An advantage of this method is that the coefficients are constant for the whole isoelectronic sequence and they depend only on the electronic state. We can note that the mixing of configurations inside one complex is taken into account by the first-order coefficients of the series considered. The complex of states means a group of configurations with the same parity and set of principal quantum numbers (2s3p + 2p3s + 2p3d, for example). The mixing between configurations of different complexes is considered by the second and other higher-order diagrams of the perturbation theory method. Breit operators are responsible for the relativistic contribution. Radiative corrections (Lamb shift) and other high-order over-relativistic contributions are also taken into account by MZ code. We will not discuss the

calculation of all $1/Z$ coefficients in detail (see an example in the papers by Manicini and Safronova (1995) and Tolstikhina *et al* (1996)).

For the $1s^22pnl'$ states of Ne^{6+}, it should be noted that the $1s^22pnl$ states for Ne^{6+} become autoionizing from $n = 7$. We certainly calculate the $1s^22snl$ and $1s^22pnl$ states together since in perturbation theory all states with one parity and with equal energy in a hydrogenic approximation must be worked out in one complex. For example, the complex of even parity with $J = 2$ includes $1s^22pnp\ ^3P_2$, $1s^22pnp\ ^1D_2$, $1s^22pnp\ ^3D_2$, $1s^22snd\ ^1D_2$, $1s^22snd\ ^3D_2$, $1s^22pnf\ ^1D_2$, $1s^22pnf\ ^3D_2$ and $1s^22pnf\ ^3F_2$ states (we consider *n*s, *n*p, *n*d and *n*f states only). All $1s^22snl$ states are not autoionizing since their energy relative to the threshold is negative, therefore we exclude these data from table 1.

Table 2. The $1s^23l3l'$ states of Ne^{6+}. The energy (eV) is relative to $1s^22p$.

Configuration	Level	a	b	c	d	e	f
$1s^23s^2$	$^1S_0$	30.43	30.13	31.03	30.50	30.01	30.51
$1s^23s3p$	$^3P_0$	33.57	33.63	34.13	33.53	33.39	33.24
$1s^23s3p$	$^1P_1$	37.30	37.16	38.03	37.31	37.12	36.95
$1s^23s3d$	$^1D_2$	37.17	36.78	37.83	37.10	37.06	36.76
$1s^23s3d$	$^3D_1$	38.31	37.74	39.13	38.42	38.17	38.15
$1s^23p^2$	$^3P_0$	39.60	39.14	40.23	39.51	39.52	39.02
$1s^23p3d$	$^3F_2$	41.49	41.68	42.33	41.54	41.73	41.03
$1s^23p3d$	$^1D_2$	41.73	41.79	42.33	41.72	41.85	41.18
$1s^23p^2$	$^1S_0$	42.74	41.89	43.43	42.55	42.72	42.07
$1s^23p^2$	$^1D_2$	42.84	42.15	43.63	42.95	42.98	42.54
$1s^23p3d$	$^3D_1$	43.71	43.53	44.43	43.74	43.81	43.33
$1s^23p3d$	$^3P_0$	44.26	43.27	44.93	44.22	44.36	43.85
$1s^23d^2$	$^3F_2$	45.64	45.16	46.43	45.91	45.94	45.39
$1s^23p3d$	$^1F_3$	46.73	46.58	48.23	46.83	46.98	46.94
$1s^23d^2$	$^1G_4$	47.53	46.98	48.83	47.71	47.82	47.49
$1s^23d^2$	$^3P_0$	47.58	47.36	49.03	48.33	48.39	48.04
$1s^23d^2$	$^1D_2$	49.20	48.23	50.63	49.11	49.05	49.39
$1s^23p3d$	$^1P_1$	49.18	48.76	50.73	49.35	49.27	49.76
$1s^23d^2$	$^1S_0$	55.44	53.8	56.93	54.83	54.93	55.91

[a] MZ code.
[b] Cowan code.
[c] Vaeck and Hansen (1989).
[d] Bachau *et al* (1990).
[e] Chen and Lin (1989).
[f] Boudjema *et al* (1991).

In table 2, we present the Auger energies of the doubly excited $1s^23l3l'$ states for Ne^{6+} calculated using MZ and Cowan codes. It should be noted that the atomic structure code of Cowan (1981) enables us to obtain results that are in good agreement with experimental energies by scaling the electrostatic Slater parameters to include correlation effects (Pindzola *et al* 1994). We use a scaling factor of 0.85. Our results obtained by the MZ and Cowan codes are compared in table 2 with results obtained by Vaeck and Hansen (1989), Bachau *et al* (1990), Chen and Lin (1989) and Boudjema *et al* (1991a). These data are listed in table 2 (a, b, c, d, e, f, respectively). We notice that there is some difference between the values in column b (Cowan code) and c (Vaeck and Hansen 1989), although both calculations were carried out using the same program written by Cowan. This discrepancy is probably due to the difference in the scaling parameter used in respective calculations. Safronova and Kato (1996) examined the influence of the scaling parameters on energy level calculations and showed that the selection

of the scaling parameters could cause discrepancies up to 0.1–0.5 eV in energy. The data in column e were obtained by the conventional configuration-interaction (CI) method developed by Chen and Lin (1989), where one fitting parameter was used for the model potential. This parameter was obtained from $1s^2nl$ data. The model potential used was that of Bachau *et al* (l990), but the fitting parameter was given in an analytical form without reference to account any experimental data. A huge number of eigenfunctions including high angular momenta was involved in these CI calculations. It can be seen from table 2 that data in column d are in good agreement with data from column e. The data in column f in table 2 were obtained using SUPERSTRUCTURE and AUTOLS codes by Boudjema *et al* (1991a). These data differ from data in columns d and e in 0.3–1 eV. The data in column a are obtained by the perturbation theory method that allows the inclusion of the correlation effect directly as the second-order contribution. The contribution of correlation effects to the energies of the $1s^23lnl'$ states has also been discussed in previous papers (Safronova *et al* 1996, Nakamura *et al* 1994, 1995, Kitazawa *et al* 1998).

4. Results

A panoramic view of the ejected electron spectra which cover the whole energy range observed is shown in figure 1 for the Ne^{8+}+ He, Ne and Ar collisions. The typical energy interval used in the horizontal axis was about 0.1 eV.

The curves in figure 1 show the reaction windows calculated using the extended classical over-barrier model (ECBM) (Niehaus 1986); these indicate the most preferable energy range for the two outermost electrons to be transferred from the target atom into the excited states $Ne^{6+}(1s^2nln'l')$ which decay to the $1s^22l$ states. The full lines indicate the reaction windows which decay to the $1s^22p$, and dotted lines those which decay to the $1s^22s$. The crossbars above the spectra show the energy regions where the following processes occur.

Coster–Kronig ($1s^22pnl \rightarrow 1s^22s$)

$$Ne^{8+}(1s^2) + B \rightarrow Ne^{6+}(1s^22pnl) + B^{2+} \rightarrow Ne^{7+}(1s^22s) + e^- + B^{2+} \tag{1}$$

Auger ($1s^23lnl' \rightarrow 1s^22l''$)

$$Ne^{8+}(1s^2) + B \rightarrow Ne^{6+}(1s^23lnl') + B^{2+} \rightarrow Ne^{7+}(1s^22l'') + e^- + B^{2+} \tag{2}$$

Auger ($1s^24lnl' \rightarrow 1s^23l''$)

$$Ne^{8+}(1s^2) + B \rightarrow Ne^{6+}(1s^24lnl'') + B^{2+} \rightarrow Ne^{7+}(1s^23l'') + e^- + B^{2+}. \tag{3}$$

We observed the ejected electrons from the three series of the excited states under our experimental conditions. In the $1s^22pnl$ energy region, we observed peaks which correspond to the states with n = 7–15. We performed energy calibration using the n = 8, 9 and 10 peaks, whose energy values are given by Boudjema *et al* (1991b) as 5.5, 7.7 and 9.3 eV. The method, which was used by Boudjema *et al* (1991b) for the energy calibration, is not clear, but these values agree well with those given by the simple Rydberg formula

$$\text{I.P.} - E(n) = \tfrac{1}{2}z^2(n-\delta)^{-2} \quad \text{(atomic unit)} \tag{4}$$

with z= 7 and $\delta \sim 0.03$, where I.P. is the $1s^22pnl$ series limit 16.0 eV and $E(n)$ is the kinetic energy of $1s^22pnl$ peak.

The peaks in the Coster–Kronig region $1s^22pnl \rightarrow 1s^22s$ are identified for n = 7–15 in the spectra in figure 2. Experimental energies for other peaks are readout from figure 2 and are given in the last column in table 3 for the respective n quantum numbers. Theoretical energies

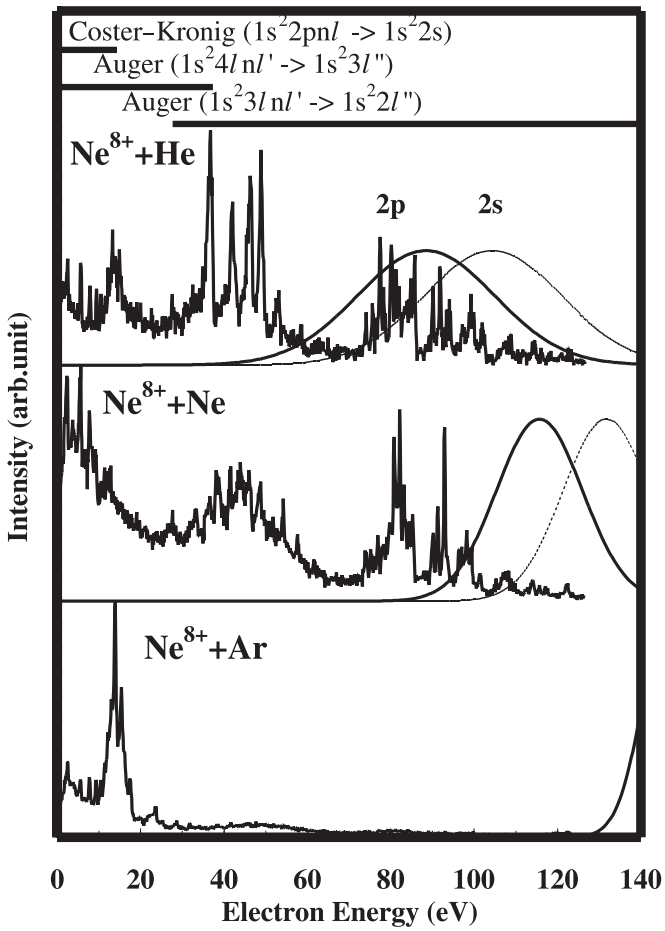

Figure 1. Ejected electron spectra from the doubly excited states of Ne^{6+**} produced by 80 keV collisions of Ne^{8+} with He, Ne and Ar. The reaction windows (Niehaus 1986) for the two outermost electrons are shown for different decay channels: full lines, $1s^22s$; dotted lines, $1s^22p$. The designations are shown in table 4.

Table 3. Coster–Kronig energies averaged over the different levels with the same configration for $Ne^{6+}(1s^22pnl)$ states (eV). Experimental data are given in the last column.

n	2p*n*s	2p*n*p	2p*n*d	2p*n*f	Exp.
7	1.8773	2.2541	2.5145	2.5400	1.78, 2.41
8	5.3292	5.5807	5.7559	5.7698	5.5
9	7.6737	7.8511	7.9740	7.9804	7.7
10	9.3365	9.4683	9.5587	9.5600	9.3
11	10.5677	10.6613	10.7281	10.7275	10.5
12	11.4935	11.5662	11.6178	11.6148	11.6
13	12.2116	12.2689	12.3096	12.3049	12.3
14	12.7796	12.8254	12.8580	12.8522	12.9
15	13.2364	13.2737	13.3001	13.2934	13.3

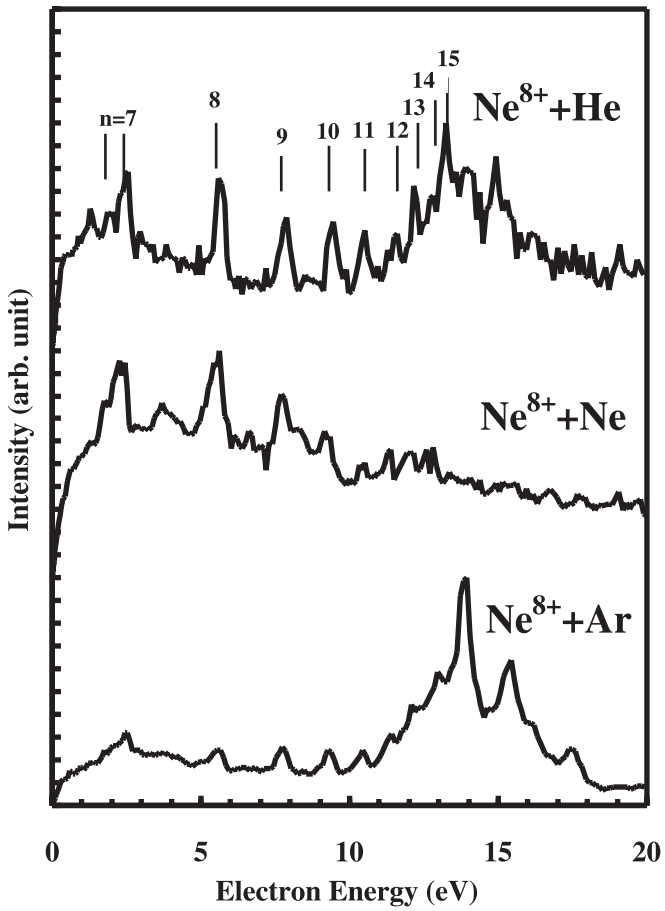

Figure 2. Coster–Kronig electron spectra emitted from the $1s^2 2pnl$ ($n = 7$–15) states of Ne^{6+**} ions produced by 80 keV collision of Ne^{8+} with He, Ne and Ar.

given in table 3 were obtained by averaging the energy values in table 1 over the different terms that have the same configuration. In table 3, experimental energies for the states with the same n quantum numbers are compared despite the difference in l quantum numbers. The theoretical energy values obtained include the shift due to the post collision interaction (PCI) effect, which is caused by the Coulomb interaction between the emitted electron and the slowly receding ionized collision partner. The PCI effect yields peak maxima at a position shift by

$$\Delta\epsilon = -Q/2V\tau(1 - V/|V - v_o|) \quad \text{(atomic unit)} \tag{5}$$

with Q the charge of the PCI-inducing collision partner, τ the lifetime of the decaying state, V the collision velocity and v_o the velocity of the ejected electron (Mack *et al* 1989).

The peaks (1.78 and 2.41 eV) are identified for $n = 7$. It should be noted that the first peak (E = 1.78 eV) corresponds to the Coster–Kronig electrons from the $1s^2 2p7s$ state and the second peak corresponds to those from $1s^2 2p7p$, $1s^2 2p7d$ and $1s^2 2p7f$. We could not observe the series limit of $1s^2 2pnl \rightarrow 1s^2 2s$ clearly, because the transition $1s^2 2pnl \rightarrow 1s^2 2s$ energetically overlaps with the $1s^2 4l5l' \rightarrow 1s^2 3p$ transition. The widths of those peaks are observed to be 0.3 eV.

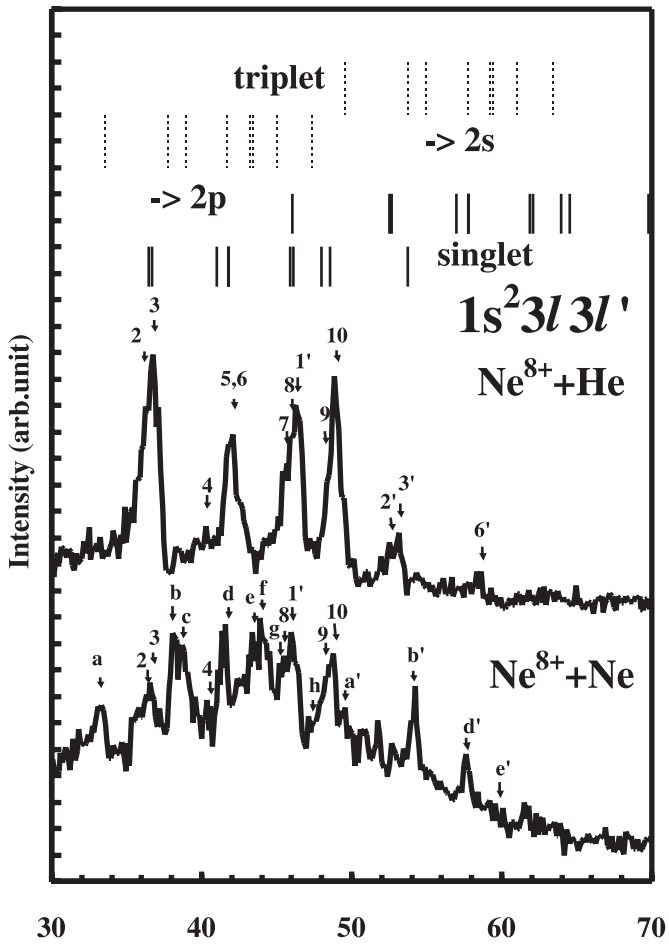

Figure 3. Ejected electron spectra from the $Ne^{6+**}(1s^2 3l3l')$ states produced by 80 keV Ne^{8+} + He and Ne collisions. The vertical lines represent the theoretical values, which include the PCI effect. The designations are shown in table 4.

Spectra of ejected electrons from the doubly excited states $Ne^{6+}(1s^2 3l3l')$ produced by collisions of 80 keV Ne^{8+} ions with He and Ne are shown in figure 3. For the Ar target, no signals were practically observed in the energy region for the $Ne^{6+}(1s^2 3lnl')$ states, as seen in figure 1. Therefore, we limit the discussion here to the cases of only the He and Ne targets. The fact that a very scarce population of the $(1s^2 3lnl')$ states occurs for the Ar target might be understood by considering that the reaction window is situated far outside this energy region.

In the case of the He target, only the singlet states of doubly excited configurations can be produced unless the collision has changed an electron spin (Nakamura *et al* 1994, 1995, Kitazawa *et al* 1998). For the Ne target, the double-electron capture process can produce both singlet and triplet doubly excited states. The spin state dependence is similar to the case of collisions of other He-like ions, O^{6+} and N^{5+}, with He and other rare-gas targets (Nakamura *et al* 1995, Kitazawa *et al* 1998).

At the top of figure 3, vertical lines show theoretical values of the electron energy. The upper two rows of lines correspond to the triplet states and the lower two rows to the singlet states, each of which consists of two groups that belong to the different decay channels. The lines labelled 2s indicate the transitions for which the final state after ejecting one electron is the $Ne^{7+}(1s^2 2s)$, and lines labelled 2p indicate the final states to be the $Ne^{7+}(1s^2 2p)$.

In figure 3, some peaks have been labelled for comparison with theory. The numerals 1, 2, 3... are used for the singlet $(1s^2 3l3l')$ states. Letters a, b, c, ... are used for the triplet $(1s^2 3l3l')$ states. Labels without a prime indicate autoionization to the $(1s^2 2p)$ and those with a prime to the $(1s^2 2s)$. Table 4 gives a comparison between theoretical energies obtained by the perturbation method (MZ code) and those from experiment. The accuracy of experimental energy values was estimated to be better than 0.2 eV. The theoretical energies have been shifted taking into account the PCI effect. In table 4, we have inserted calculated data for branching ratios (c) and (d) for the decay channels $1s^2 2p$ and $1s^2 2s$, respectively. Auger widths are also included in units of 10^{13} s^{-1}. The data c1, d1 and e1 are calculated using the Cowan code.

In the case of the He target, all singlet states labelled 2 to 10 are identified for the decay channel $1s^2 2p$ except for the imaginary line number (1). The absence of line 1 is well explained by the theoretical results that the branching ratio of the $(1s^2 3s^2)$ $^1S_0$ state to the $1s^2 2p$ decay channel, 0.002, is negligibly small compared with the other decay channel $1s^2 2s$, 0.998. Instead of line 1, the autoionization $1s^2 3s^2$ $^1S_0 \rightarrow 1s^2 2s$ produces line $1'$ clearly, as shown in figure 3. For the decay channel $1s^2 2s$, lines $1'$, $2'$, $3'$ and $6'$ are identified. Intensity ratios of corresponding lines without a prime to those with a prime, for instance intensity ratio of line 2 to line $2'$, reflect reasonably the theoretical branching ratios. No traces for imaginary $9'$ and $10'$ lines are observed, reflecting that the corresponding branching ratios to the $1s^2 2s$ channel are negligibly small.

In the case of the Ne target, for the decay channel $1s^2 2p$, eight peaks for triplet states (labelled a–h) were identified, in addition to six peaks for singlet states (labelled 2–10) as shown in figure 3. For the decay channel $1s^2 2s$, four peaks (a'–e') were identified. In the whole energy range, lines due to triplet states prevail over those due to singlet states.

Agreement between experimental and theoretical energy values is found to be within 0.3 eV except for several peaks, as seen in figure 3 and table 4.

Spectra of ejected electrons from the configuration of $Ne^{6+}(1s^2 3l4l')$ produced in collisions of 80 keV Ne^{8+} ions with He and Ne targets are shown in figure 4. The labelling scheme follows that of figure 3, but for peaks of the $1s^2 3l4l'$ manifold. In table 5, results of theoretical calculations for state energy, branching ratio and Auger width are tabulated for the $1s^2 3l4l'$ configuration following the same scheme as that of table 4. Table 5 also gives an identification of the $Ne^{6+}(1s^2 3l4l')$ spectra. It is more difficult to identify these spectra than is the case with $Ne^{6+}(1s^2 3l3l')$, because the $1s^2 3l4l'$ manifold comprises 56 terms in a 30 eV interval, whereas the $1s^2 3l3l'$ manifold includes only 19 terms in the same energy interval.

For the He target, we succeeded in identifying 15 peaks due to singlet states for the $1s^2 2p$ decay channel, and 13 peaks for the $1s^2 2s$ decay channel. Absence of line $4'$ is well explained by the prediction that the branching ratio to the $1s^2 2s$ channel for the $(1s^2 3p4p)^1P_1$ state has to be zero. A part of the energy region for the $1s^2 2s$ decay channel overlap with some peaks attributable to the Auger decay $Ne^{6+}(1s^2 3l5l') \rightarrow 1s^2 2p$ as indicated by I to IV in figure 4.

In the case of the Ne target, if singlet and triplet states are formed with almost the same probabilities as for the $1s^2 3l4l'$ configuration, the emitted electron spectrum probably becomes very complicated; but, in fact, we obtain a rather simple spectrum compared with the He target case, as shown in figure 4. Though the $1s^2 3l4l'$ formation by the collision with the Ne target does not exist in the centre region of the reaction window, it still remains in the tail region (see figure 1), so we can expect that the two outermost electron transfer process is more probable

Table 4. $1s^2 3l3l'$ states for Ne^{6+}. The energy(eV) is relative to the $1s^2 2p$(a) and $1s^2 2s$(b) states, branching ratios for $1s^2 2p$(c) and $1s^2 2s$(d) channels and Auger widths in 10^{13} s^{-1}. The PCI effect is included on the energy. Experimental data are given in the column Exp. a1, b1, c1, d1, e1, this work; a2, b2, c2, d2, e2, Boudjema *et al* (1991a); a3, b3, Bachau *et al* (1990).

		Auger widths (e)		Branching ratio (c)		Energy (a)				
Configuration	Level	e1	e2	c1	c2	a1	a2	a3	Exp.	Peak
$1s^2 3l3l' \rightarrow 1s^2 2p$										
$3s^2$	$^1S_0$	9.62	13.3	0.002	0.018	30.03	29.86	30.16	–	(1)
3s3p	$^3P_0$	11.21	13.7	0.546	0.546	33.51	33.05	32.85	33.3	a
3s3p	$^1P_1$	42.72	48.5	0.67	0.661	36.68	36.06	35.66	36.8	3
3s3d	$^1D_2$	26.06	32.2	0.603	0.704	36.49	36.24	35.94	36.2	2
3s3d	$^3D_1$	3.15	3.46	0.368	0.355	37.70	38.26	37.96	38.1	b
$3p^2$	$^3P_0$	21.69	26.4	1	1	38.89	38.80	38.40	38.7	c
3p3d	$^3F_2$	0.212	0.01	0.76	0.864	41.68	41.40	40.90	41.6	d
3p3d	$^1D_2$	1.77	1.64	1	1	41.77	41.58	41.08	41.8	5
$3p^2$	$^1S_0$	76.85	89.2	0.884	0.894	41.00	40.28	39.58	40.3	4
$3p^2$	$^1D_2$	29.4	34.5	0.638	0.598	41.81	42.00	41.50	42.1	6
3p3d	$^3D_1$	13.01	15.2	1	1	43.38	43.22	42.92	43.7	f
3p3d	$^3P_0$	7.27	7.71	0.941	0.930	43.19	43.91	43.61	43.4	e
$3d^2$	$^3F_2$	13.72	16.0	1	1	45.00	45.41	44.91	45.4	g
3p3d	$^1F_3$	41.66	43.7	0.884	0.897	46.09	45.58	45.88	45.9	8
$3d^2$	$^1G_4$	89.71	96.9	0.863	0.895	45.92	45.15	44.85	45.4	7
$3d^2$	$^3P_0$	0.863	0.837	1	1	47.35	48.19	47.89	–	h
$3d^2$	$^1D_2$	22.08	20.4	0.998	0.993	47.97	48.46	48.76	48.7	9
3p3d	$^1P_1$	19.08	21.0	0.999	0.985	48.53	48.75	49.15	48.9	10
$3d^2$	$^1S_0$	3.52	2.70	0.716	0.743	53.76	54.37	55.77	–	–

		Auger widths (e)		Branching ratio (d)		Energy (b)				
Configuration	Level	e1	e2	d1	d2	b1	b2	b3	Exp.	Peak
$1s^2 3l3l' \rightarrow 1s^2 2s$										
$3s^2$	$^1S_0$	9.62	13.3	0.998	0.982	46.04	45.86	46.16	46.3	1′
3s3p	$^3P_0$	11.21	13.7	0.454	0.454	49.52	49.06	48.86	49.5	a′
3s3p	$^1P_1$	42.72	48.5	0.33	0.339	52.66	52.03	51.63	53.1	3′
3s3d	$^1D_2$	26.06	32.2	0.397	0.296	52.48	52.23	51.93	52.5	2′
3s3d	$^3D_1$	3.15	3.46	0.632	0.645	53.72	54.28	53.98	54.2	b′
$3p^2$	$^3P_0$	21.69	26.4	0	0	54.89	–	–	–	–
3p3d	$^3F_2$	0.212	0.01	0.24	0.136	57.70	57.42	56.92	57.6	d′
3p3d	$^1D_2$	1.77	1.64	0	0	57.79	–	–	–	–
$3p^2$	$^1S_0$	76.85	89.2	0.116	0.106	56.95	56.21	55.51	–	–
$3p^2$	$^1D_2$	29.4	34.5	0.362	0.402	57.80	57.99	57.49	58.1	6′
3p3d	$^3D_1$	13.01	15.2	0	0	59.39	–	–	–	–
3p3d	$^3P_0$	7.27	7.71	0.059	0.070	59.20	59.92	59.62	59.2	e′
$3d^2$	$^3F_2$	13.72	16.0	0	0	61.01	–	–	–	–
3p3d	$^1F_3$	41.66	43.7	0.116	0.103	62.07	61.57	61.87	–	–
$3d^2$	$^1G_4$	89.71	96.9	0.137	0.105	61.87	61.10	60.80	–	–
$3d^2$	$^3P_0$	0.863	0.84	0	0	63.37	–	–	–	–
$3d^2$	$^1D_2$	22.08	20.4	0.002	0.007	63.97	64.46	64.76	–	9′
3p3d	$^1P_1$	19.08	21.0	0.001	0.015	64.54	64.75	65.15	–	10′
$3d^2$	$^1S_0$	3.52	2.70	0.284	0.257	69.77	70.39	71.79	–	–

Table 5. $1s^2 3l4l'$ states for Ne^{6+}. The energy (eV) is relative to the $1s^2 2p$(a) and $1s^2 2s$(b) states, branching ratios for $1s^2 2p$(c) and $1s^2 2s$(d) channels and Auger widths in 10^{13} s^{-1} (e). Experimental data are given in the column Exp. a1, b1, this work; a2, b2, Bachau *et al* (1990); a3, b3, Boudjema *et al* (1991a).

				Energy (a)				
Configuration	Level	Auger widths (e)	Branching ratio (c)	a1	a2	a3	Exp.	Peak
$1s^2 3l4l' \rightarrow 1s^2 2p$								
3s4s	$^3S_1$	0.212	0.005	71.59	71.94	–		
3s4s	$^1S_0$	8.27	0.020	72.44	72.88	72.59		
3s4p	$^1P_1$	2.28	0.318	72.77	73.73	73.57	74.1	1
3s4p	$^3P_0$	5.98	0.425	73.17	74.26	–	73.8	a
3s4d	$^3D_1$	0.934	0.121	74.98	75.31	–	75.2	b
3s4d	$^1D_2$	7.38	0.361	75.13	75.54	75.30	75.6	2
3s4f	$^3F_2$	0.379	0.027	77.02	76.96	–	76.9	c
3p4s	$^3P_0$	2.86	0.806	77.01	76.80	–	76.9	c
3s4f	$^1F_3$	4.60	0.950	76.71	77.23	76.64	76.6	3
3p4s	$^1P_1$	28.0	0.677	77.83	77.68	76.83		
3p4p	$^1P_1$	0.208	1	77.71	77.94	77.60	77.5	4
3p4p	$^3D_1$	1.11	0.482	78.06	78.43	–		
3d4s	$^1D_2$	14.1	0.889	77.89	78.21	77.72	78.3	5
3p4p	$^3P_0$	15.9	1	78.74	79.08	–		
3p4p	$^3S_1$	0.450	0.822	78.58	78.99	–		
3p4d	$^3D_1$	0.908	1	79.42	79.22	–	79.7	d
3p4d	$^1F_3$	0.0838	0.911	79.85	79.71	79.40	80.1	6
3d4s	$^3D_1$	0.105	0.307	79.35	79.92	–		
3p4d	$^1D_2$	1.64	1	80.01	79.86	79.48	80.1	6
3p4d	$^1P_1$	1.22	0.995	80.24	80.16	79.98	80.1	6
3p4d	$^3F_2$	0.137	0.198	80.56	80.32	–	80.8	e
3p4f	$^1F_3$	0.283	1	80.32	80.76	80.30	80.8	
3p4f	$^3G_3$	0.333	0.864	80.45	80.83	–	80.8	e
3d4p	$^1D_2$	0.918	1	81.01	80.89	80.39		
3p4d	$^3P_0$	2.33	0.995	81.19	81.20	–		
3p4f	$^3F_2$	0.270	1	80.71	81.13	–		
3d4p	$^3F_2$	4.35	0.751	81.35	81.37	–	81.6	f
3p4p	$^1S_0$	50.8	0.913	80.16	80.62	79.23		
3p4p	$^1D_2$	18.4	0.592	80.79	81.30	80.56	81.2	7
3d4d	$^1F_3$	0.347	1	81.17	81.74	81.60	81.2	7
3d4d	$^3D_1$	0.0863	0.937	81.37	81.95	–	81.6	f
3d4p	$^3D_1$	8.25	1	81.92	81.87	–		
3d4d	$^1P_1$	0.0252	1	81.82	82.56	82.40	82.0	8
3d4d	$^3G_3$	1.43	0.961	81.83	82.33	–		
3d4p	$^3P_0$	2.85	0.919	82.29	82.30	–		
3d4f	$^1G_4$	0.740	1	82.46	82.40	82.29	82.8	10
3d4f	$^3H_4$	–	–	–	–	–		
3p4f	$^1G_4$	26.0	0.806	81.83	81.94	81.76	82.3	9
3p4f	$^3D_1$	0.626	0.982	82.49	83.10	–	83.2	g
3d4f	$^3F_2$	0.539	0.983	83.28	83.35	–	83.2	g
3d4f	$^3F_2$	8.46	1	82.66	83.26	–	83.2	g
3d4f	$^1D_2$	0.268	1	83.62	83.82	83.70	83.9	12
3d4d	$^3S_1$	0.103	0.642	83.13	83.98	–		
3d4f	$^3G_3$	1.34	1	84.08	84.28	–		
3p4f	$^1D_2$	2.50	0.702	83.29	83.49	83.47	83.4	11

Table 5. Continued.

				Energy (a)				
Configuration	Level	Auger widths (e)	Branching ratio (c)	a1	a2	a3	Exp.	Peak
3d4p	$^1F_3$	23.0	0.867	83.70	83.43	83.20	83.9	12
3d4f	$^1F_3$	1.88	0.914	85.37	85.27	86.08	85.8	15
3d4d	$^3P_0$	0.792	1	83.79	84.45	–		
3d4f	$^3D_1$	–	–	–	–	–		
3d4d	$^1G_4$	28.8	0.954	84.25	84.52	84.32	84.8	13
3d4f	$^3P_0$	0.0709	0.649	85.13	85.45	–	85.2	i
3d4d	$^1D_2$	9.71	0.976	84.50	84.84	84.87	84.8	13
3d4p	$^1P_1$	12.3	0.999	84.92	84.43	84.64	85.4	14
3d4f	$^1H_5$	–	–	–	–	–		
3d4f	$^1P_1$	0.184	0.994	86.69	86.77	87.60		
3d4d	$^1S_0$	4.96	0.686	87.09	87.02	87.63		

				Energy (a)				
Configuration	Level	Auger widths (e)	Branching ratio (d)	b1	b2	b3	Exp.	Peak
$1s^2 3l4l' \rightarrow 1s^2 2s$								
3s4s	$^3S_1$	0.212	0.995	87.61	87.96	–		
3s4s	$^1S_0$	8.27	0.980	88.46	88.90	88.61	89.0	
3s4p	$^1P_1$	2.28	0.682	88.79	89.75	89.59	90.1	1′
3s4p	$^3P_0$	5.98	0.575	89.19	90.28	–	90.2	a′
3s4d	$^3D_1$	0.934	0.879	91.00	91.33	–	91.3	b′
3s4d	$^1D_2$	7.38	0.639	91.15	91.56	91.32	91.7	2′
3s4f	$^3F_2$	0.379	0.976	93.03	92.97	–		c′
3p4s	$^3P_0$	2.86	0.194	93.03	92.82	–		c′
3s4f	$^1F_3$	4.60	0.050	92.73	93.25	92.66	92.7	3′
3p4s	$^1P_1$	28.0	0.323	93.84	93.69	92.84		
3p4p	$^1P_1$	0.208	0	93.73	93.96	–	93.4	4′
3p4p	$^3D_1$	1.11	0.518	94.08	94.45	–		
3d4s	$^1D_2$	14.1	0.111	93.90	94.22	93.73	94.3	5′
3p4p	$^3P_0$	15.9	0	94.76	95.10	–		
3p4p	$^3S_1$	0.450	0.178	94.60	95.01	–		
3p4d	$^3D_1$	0.908	0	95.44	95.24	–	95.8	d′
3p4d	$^1F_3$	0.0838	0.089	95.87	95.73	95.42	95.9	6′
3d4s	$^3D_1$	0.105	0.693	95.37	95.94	–		
3p4d	$^1D_2$	1.64	0	96.03	95.88	–		
3p4d	$^1P_1$	1.22	0.005	96.26	96.18	96.00		
3p4d	$^3F_2$	0.137	0.802	96.58	96.34	–		
3p4f	$^1F_3$	0.283	0	96.34	96.78	–		
3p4f	$^3G_3$	0.333	0.136	96.47	96.85	–	96.4	e′
3d4p	$^1D_2$	0.918	0	97.03	96.91	–		
3p4d	$^3P_0$	2.33	0.005	97.21	97.22	–	96.4	e′
3p4f	$^3F_2$	0.270	0	96.73	97.15	–		
3d4p	$^3F_2$	4.35	0.249	97.37	97.39	–	97.0	f′
3p4p	$^1S_0$	50.8	0.087	96.16	96.62	95.24		
3p4p	$^1D_2$	18.4	0.408	96.80	97.31	96.57	97.2	7′
3d4d	$^1F_3$	0.347	0	97.19	97.76	–	97.2	7′
3d4d	$^3D_1$	0.0863	0.063	97.39	97.97	–	97.0	f′
3d4p	$^3D_1$	8.25	0	97.94	97.89	–		
3d4d	$^1P_1$	0.0252	0	97.84	98.58	–	98.0	8′
3d4d	$^3G_3$	1.43	0.039	97.85	98.35	–		

Table 5. Continued.

				Energy (a)				
Configuration	Level	Auger widths (e)	Branching ratio (d)	b1	b2	b3	Exp.	Peak
3d4p	$^3P_0$	2.85	0.081	98.31	98.32	–		
3d4f	$^1G_4$	0.740	0	98.48	98.42	–	98.8	10′
3d4f	$^3H_4$		–	–	–	–	–	
3p4f	$^1G_4$	26.0	0.194	97.84	97.95	97.77	98.3	9′
3p4f	$^3D_1$	0.626	0.018	98.51	99.12	–	98.2	g′
3d4f	$^3F_2$	0.539	0.017	99.30	99.37	–	98.2	g′
3d4d	$^3F_2$	8.46	0	98.68	99.28	–	98.2	g′
3d4f	$^1D_2$	0.268	0	99.64	99.84	–	99.9	12′
3d4d	$^3S_1$	0.103	0.358	99.15	100.00	–		
3d4f	$^3G_3$	1.34	0	100.10	100.30	–		
3p4f	$^1D_2$	2.50	0.298	99.31	99.51	99.49	99.2	11′
3d4p	$^1F_3$	23.0	0.133	99.71	99.44	99.21	99.9	12′
3d4f	$^1F_3$	1.88	0.086	101.38	101.28	102.09	101.9	15′
3d4d	$^3P_0$	0.792	0	99.81	100.47	–		
3d4f	$^3D_1$	–	–	–	–	–		
3d4d	$^1G_4$	28.8	0.046	100.26	100.53	100.33	100.7	13′
3d4f	$^3P_0$	0.0709	0.351	101.15	101.47	–	101.3	h′
3d4d	$^1D_2$	9.71	0.024	100.52	100.86	100.89	100.7	13′
3d4p	$^1P_1$	12.3	0.000	100.93	100.44	100.65	101.3	14′
3d4f	$^1H_5$	–	–	–	–	–		
3d4f	$^1P_1$	0.184	0.006	102.71	102.79	103.62		
3d4d	$^1S_0$	4.96	0.314	103.11	103.04	103.65		

than other types of electron transfer, and that triplet states are dominantly formed as in the case of N^{5+} + Ar and O^{6+} + Ne collisions. For this reason, we identified most peaks in the Ne target spectrum as triplet ones. Nine peaks (labelled a–i) caused by triplet states have been identified for the $1s^2 2p$ decay channel. Peaks labelled a′–i′ were also identified for the $1s^2 2s$ decay channel. For singlet states, only three peaks, 1, 6 and 1′, were identified.

5. Discussion

As we already noted in figure 3, the reaction windows calculated for the capture of the two outermost electrons from the target do not always indicate properly the energy region where the double-electron capture processes concerned take place. For instance, in the case of the Ne target, as shown in figure 5, the reaction windows for the $1s^2 3l3l'$ states for the capture of two outermost electrons from Ne target, labelled a and b, are situated perfectly outside of the energy region of the ejected electron spectrum, indicated by $(1s^2 3l3l')$ in figure 5.

We investigate possible processes where the capture of two electrons from the inner sites of the target atom takes place. We use the (j) string scheme by Niehaus (1986) to express each process. In this string, we indicate by the position of the index of an electron in order of the original binding energy, and '1' or '0' in the string signifies whether it has been captured by the projectile ion or remains on the target. For example, the string $(j) = (10100000)$ characterizes a process in which the electron of index 1 of original binding energy I_1 on the target, and the electron of index 3 with original binding energy I_3 are captured by the projectile ion, while the other electrons remain on the target. The process where the outermost two electrons are captured is expressed by the string $(j) = (11000000)$.

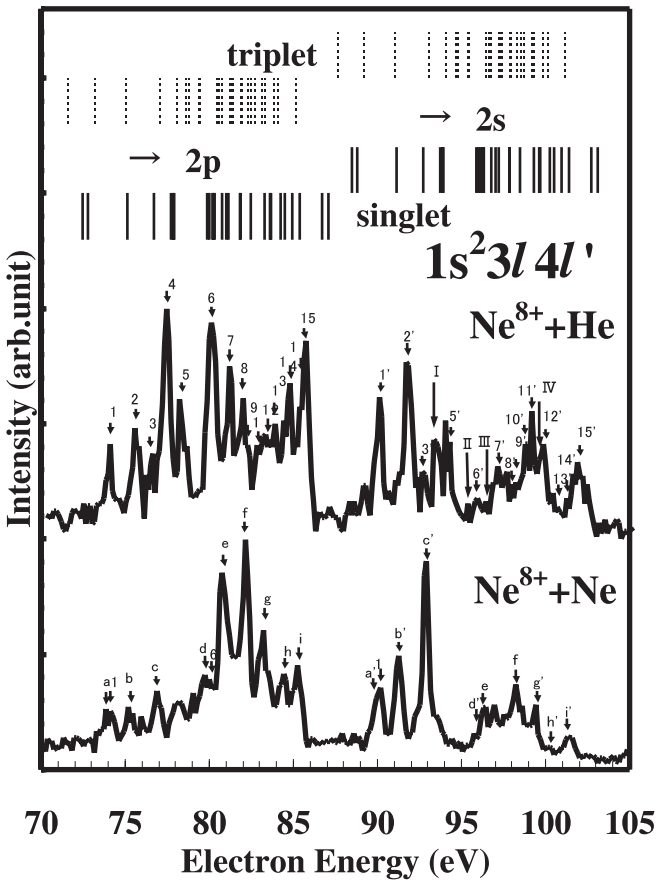

Figure 4. Ejected electron spectra from the $Ne^{6+**}(1s^2 3l4l')$ states produced by 80 keV Ne^{8+} + He and Ne collisions. The vertical lines represent the theoretical values, which include the PCI effect. The designations are shown in table 5.

We calculated the reaction windows for five different cases of (j) strings for the production of the ejected electron spectrum due to the $1s^2 3l3l'$ states, using the extended classical over-barrier model (Niehaus 1986). Each (j) string, i.e. capture process, has two different decay channels, the $1s^2 2s$ and $1s^2 2p$; therefore, two curves are calculated for each string. Ten curves of reaction windows for the five different (j) strings are drawn in figure 5. It is worth noting that the energy region over which the reaction window has considerable intensity moves closer to the energy range of the spectrum as the index of the electron to be captured becomes higher. For instance, the reaction windows for the $(j) = (10001000)$, curves g and h, are situated much closer to the $1s^2 3l3l'$ region than are the windows for the $(j) = (11000000)$, curves a and b, as seen in figure 5. Although cross sections for the former are much smaller than for the latter, the possibility of capture processes where inner electrons are involved should not be ignored. Thus the results of calculations based on the (j) string analysis suggest that the participation of the inner electrons of the target atom in the double-electron capture processes by highly charged ions has to be considered more seriously. In addition to the above discussion, we must consider the effect of multi-electron capture and Auger cascade from states with three or more electron excited states. These Auger processes should eject low-energy electrons, but, from figures 1

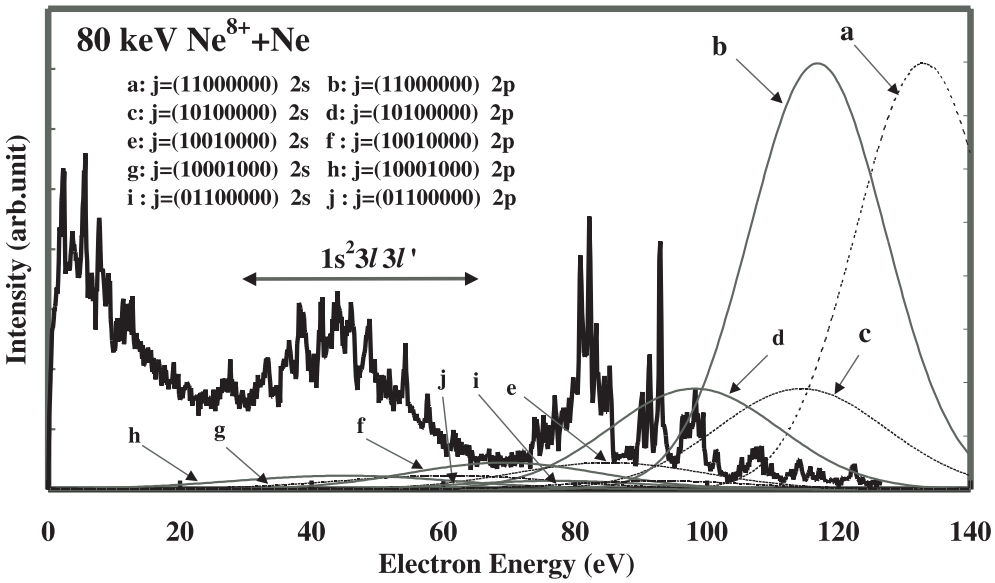

Figure 5. The reaction windows (Niehaus 1986) for five sets of (j) strings for the $1s^2 3l3l'$ states are shown in the ejected electron spectrum from the $Ne^{6+**}(1s^2 3ln'l')$ states produced by 80 keV Ne^{8+} + Ne collisions. Each set has two curves for different decay channels: dotted curves, $1s^2 2s$; full curves, $1s^2 2p$.

and 2, we can recognize that there are not very pronounced peaks corresponding to such Auger processes in low-energy regions of the Ne target spectra. Of course, we need coincidence measurements between ejected electrons and target ions to confirm the above discussion.

6. Summary

We have measured ejected electron spectra produced by double-electron capture in collisions of 80 keV Ne^{8+} ions with He, Ne and Ar by means of high resolution electron spectroscopy of a zero degree arrangement. Spectral peaks due to the Coster–Kronig process $Ne^{6+}(1s^2 2pnl) \rightarrow Ne^{7+}(1s^2 2s)$ and those due to the Auger processes from $Ne^{6+}(1s^2 3l3l')$ and $Ne^{6+}(1s^2 3l4l')$ states to $Ne^{7+}(1s^2 2p)$ and $Ne^{7+}(1s^2 2s)$ have been identified by comparing them with calculated values of energies and by considering the rules for the spin state formation and the calculated branching ratios. Theoretical data were calculated using the atomic structure code of Cowan and the perturbation theory method (MZ code). For the He target, only singlet states are formed. In contrast, for the Ne target triplet states were more prominent than singlet ones. For the Ar target, only minute signals were observed in the present manifold.

With the aid of the (j) string analysis in the extended classical over-barrier model (Niehaus l986), we discussed the importance of the participation of inner electrons in the process of double-electron capture by highly charged ion multi-electron atom targets.

Acknowledgments

One of the authors (SK) thanks Dr Ichihara (JAERI) for many recommendations in understanding the theoretical approach and thanks Dr Ichimura (ISAS) for advice in analysing the experimental results.

References

Bachau H, Glan P, Martin F, Riera A and Yanez M 1990 *At. Data Nucl. Data Tables* **44** 305–48

Bonnet J J, Fleury A, Bonnefoy M, Politis M F, Chassevent M, Bliman S, Dousson S and Hitz D 1985 *J. Phys. B: At. Mol. Phys.* **18** L23–7

Boudjema M, Cornille M, Dubau J, Moretto-Capelle P, Bordenave-Montesquieu A, Benoit-Cattin P and Gleizes A 1991a *J. Phys. B: At. Mol. Phys.* **24** 1695–712

——1991b *J. Phys. B: At. Mol. Phys.* **24** 1713–37

Chen Z and Lin C D 1989 *J. Phys. B: At. Mol. Opt. Phys.* **22** 2875–86

Cowan R D 1981 *The Theory of Atomic Structure and Spectra* (Berkeley, CA: University of California Press)

Kanai Y *et al* 1995 *Nucl. Instrum. Methods* B **98** 81–4

Kitazawa S, Iemura K, Ohtani S, Koide M, Suzuki H, Sekiguchi M, Takayanagi T, Machida S and Wakiya K 1997 *Phys. Scr.* T **73** 207–8

Kitazawa S *et al* 1998 *J. Phys. B: At. Mol. Opt. Phys.* **31** 3233–43

Mack A and Niehaus A 1987 *Nucl. Instrum. Methods* B **23** 116–9

Mack M, Nijland J H, Straten P v d, Niehaus A and Morgenstern R 1989 *Phys. Rev.* A **39** 3846–54

Mancini R C and Safronova U I 1995 *J. Phys. B: At. Mol. Opt. Phys.* **28** 3469–84

Nakamura N *et al* 1994 *J. Phys. B: At. Mol. Opt. Phys.* **27** L785-93

——1995 *J. Phys. B: At. Mol. Opt. Phys.* **28** 4743–58

Niehaus A 1986 *J. Phys. B: At. Mol. Phys.* **19** 2925–37

Pindzola M S *et al* 1994 *Phys. Rev.* A **49** 933–8

Safronova M S, Safronova U I, Namakura N and Ohtani S 1996 *Phys. Scr.* **53** 689–99

Safronova U I and Senashenko V S 1984 *Theory of Spectra of Multicharged Ions* (Moscow: Energoatomizdat)

Safronova U I and Kato T 1996 *Phys. Scr.* **53** 461–72

Sakaue H A *et al* 1990 *J. Phys. B: At. Mol. Opt. Phys.* **23** L401–5

Tolstikhina I Yu, Tawara H, Safronova U I, Imai M, Sataka M, Kawatsura K, Komaki K and Yamazaki Y 1996 *Phys. Scr.* **54** 188–96

Vaeck N and Hansen J E 1989 *J. Phys. B: At. Mol. Opt. Phys.* **22** 3137–53